PHYSICAL REVIEW A **84**, 011805(R) (2011)

Coupling of a single diamond nanocrystal to a whispering-gallery microcavity: Photon transport benefitting from Rayleigh scattering

Yong-Chun Liu, Yun-Feng Xiao,* Bei-Bei Li, Xue-Feng Jiang, Yan Li, and Qihuang Gong†
State Key Lab for Mesoscopic Physics, School of Physics, Peking University, Beijing 100871, People's Republic of China
(Received 17 September 2010; published 25 July 2011)

We study the Rayleigh scattering induced by a diamond nanocrystal in a whispering-gallery-microcavity–waveguide coupling system and find that it plays a significant role in the photon transportation. On the one hand, this study provides insight into future solid-state cavity quantum electrodynamics aimed at understanding strong-coupling physics. On the other hand, benefitting from this Rayleigh scattering, effects such as dipole-induced transparency and strong photon antibunching can occur simultaneously. As a potential application, this system can function as a high-efficiency photon turnstile. In contrast to B. Dayan *et al*. [Science **319**, 1062 (2008)], the photon turnstiles proposed here are almost immune to the nanocrystal's azimuthal position.

DOI: 10.1103/PhysRevA.84.011805 PACS number(s): 42.50.Ar, 78.35.+c, 42.50.Pq, 78.67.Bf

Cavity quantum electrodynamics (CQED) studies light-matter interactions inside a resonator, which offers an ideal platform for quantum optics [1]. Tremendous progress has been made by coupling single dipoles to different microcavities (for a review, see [2]). Among them, the whispering-gallery mode (WGM) type of microcavity [3] is the most promising due to its extremely high Q factor, small mode volume, excellent scalability, and ease of use for low-loss transport of nonclassical states using an optical fiber [4,5]. On the other hand, nitrogen-vacancy (NV) centers have recently emerged as an important candidate for quantum information processing because they possess long-lived spin triplets at room temperature [6,7]. A combination of high-Q WGM microcavities and NV centers represents a promising solid-state CQED system, which has attracted much attention recently [4,5,8].

One of the distinct properties of WGMs is that they are traveling modes, unlike standing modes in a Fabry-Pérot cavity. In other words, WGM microcavities typically support twin modes, clockwise (cw) and counterclockwise (ccw) propagating modes with a degenerate frequency. In this Rapid Communication, we investigate the interaction of twin WGMs coupled to a NV center in a diamond nanocrystal. We find that not only the dipole transition of the NV center but also the Rayleigh scattering by the nanocrystal itself play significant roles in the coupled system. Thus, strong-coupling conditions in such a CQED system should be redefined. More importantly, nonclassical effects are predicted, benefitting from the nanocrystal scattering. Dipole-induced transparency (DIT) [9] appears in the presence of strong Rayleigh scattering, accompanying strong photon antibunching in transmitted fields. Moreover, high-efficiency photon turnstiles can be implemented that are almost immune to the azimuthal position of the nanocrystal.

Figure 1 describes the present coupling system. A diamond nanocrystal embodying a single NV center is located on the surface of a microtoroidal cavity [10]. A tapered fiber is used to couple light with frequency ω_p in and out of the microcavity. Under the rotating-wave approximation, the Hamiltonian of the coupled system can be written as ($\hbar = 1$)

$$\begin{aligned} H &= H_0 + H_1 + H_2, \\ H_0 &= \omega_e|e\rangle\langle e| + \sum_m \omega_c a_m^\dagger a_m + \sum_{k=1}^{3}\sum_j \omega_{kj} b_{kj}^\dagger b_{kj}, \\ H_1 &= \sum_m G_m a_m^\dagger \sigma_- + \sum_j G_j b_{1j}^\dagger \sigma_- + \text{H.c.}, \\ H_2 &= \sum_{m,m'} g_{m,m'} a_m^\dagger a_{m'} + \sum_j (g_{\text{cw},j} a_{\text{cw}}^\dagger b_{2j} + \text{H.c.}) \\ &\quad + \sum_j (g_{\text{ccw},j} a_{\text{ccw}}^\dagger b_{3j} + \text{H.c.}). \end{aligned} \tag{1}$$

Here summation indices (m,m') run through cw and ccw modes; a_m and b_{kj} $(k = 1,2,3)$ denote annihilation operators of the cavity and the reservoir modes, respectively; $\sigma_- = |g\rangle\langle e|$ and $\sigma_+ = |e\rangle\langle g|$ stand for the descending and ascending operators of the dipole transition at the zero-phonon line. The Hamiltonian H_0 describes the free evolution of the system consisting of the NV center, WGMs, and reservoir modes, with frequencies ω_e, ω_c, and ω_{kj}, respectively. The first (second) term in H_1 characterizes the dipole interactions between the NV center and WGM (reservoir modes), with the coupling strength G_m (G_j). The first term in H_2 describes the nanocrystal-induced scattering into the same $(m = m')$ or the counterpropagating $(m \neq m')$ WGM fields with strengths $g_{m,m'}$, while the second term represents the WGM-reservoir scattering coefficients $g_{m,j}$.

In the full quantum theory, the coherent coupling strengths G_m and G_j can be calculated by $G_m \equiv G = \mu[\omega_c/(2\hbar\varepsilon_0\varepsilon_s V_c)]^{1/2} f_c(\vec{r})$ and $G_j = \mu[\omega_{1j}/(2\hbar\varepsilon_0\varepsilon_s V_{1j})]^{1/2}$, where $\mu = 2.74 \times 10^{-29}$ C m represents the dipole moment of the NV center transition. ε_0 is the electric permittivity of the vacuum and $\varepsilon_s = 1$ denotes the relative permittivity of the surrounding medium (vacuum here). V_c and V_{1j} are the quantized volumes of the cavity and the reservoir modes interacting with the dipole, respectively. $f_c(\vec{r}) = |E(\vec{r})/E_{\max}|$ is the normalized field distribution function of the WGMs. For a subwavelength nanocrystal, the above scattering interaction can be modeled in a dipole approximation where the electric field of the

*Corresponding author: yfxiao@pku.edu.cn; URL: http://www.phy.pku.edu.cn/~yfxiao/index.html
†qhgong@pku.edu.cn

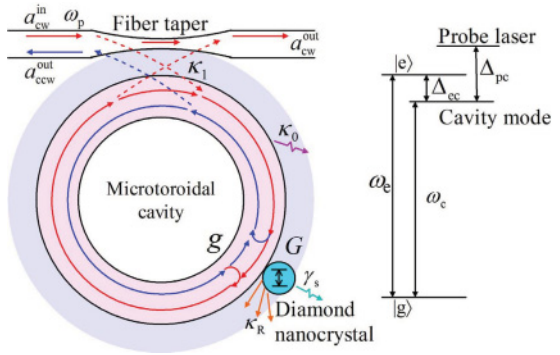

FIG. 1. (Color) Schematic illustration of the nanocrystal-microcavity-waveguide coupling system.

input wave (either WGMs or reservoir modes) induces a dipole moment in the scatterer, namely, a *scattering-induced dipole*. In the case of elastic Rayleigh scattering, the coupling strengths are $g_{m,m'} \equiv -g = -\alpha f_c^2(\vec{r})\omega_c/(2V_c)$ and $g_{m,j} \equiv -g_R = -\alpha f_c(\vec{r})\omega_c(\hat{n}_m \cdot \hat{n}_{k,j})/(4V_cV_{k,j})^{1/2}$ ($m = \text{cw}$, $k = 2$ or $m = \text{ccw}$, $k = 3$) [11]. Here $\alpha = 4\pi R^3(\varepsilon_d - \varepsilon_s)/(\varepsilon_d + 2\varepsilon_s)$ is the polarizability for the spherical nanocrystal with radius R, where $\varepsilon_d = 2.4^2$ denotes the electric permittivity of the diamond. $\hat{n}_m$ and $\hat{n}_{k,j}$ are unit vectors of the fields.

We can use the same format for both the NV-center–reservoir and WGM-reservoir coupling interactions. By using the Weisskopf-Wigner approximation, the coupling of the NV center to the reservoir can be regarded as a decay of the excited state, that is, the well-known spontaneous emission with rate γ_s, while the scattering of WGMs to the reservoir can be modeled by an energy damping of the WGMs, with the damping rate $\kappa_R = \alpha^2 f_c^2(\vec{r})\varepsilon_s^{3/2}\omega_c^4/(6\pi c^3 V_c)$ [11], where c is the speed of light in vacuum. Transforming traveling to standing modes, $a_\pm = (a_{\text{cw}} \pm a_{\text{ccw}})/\sqrt{2}$, the equations of motion for the coupled system are given by [12]

$$\frac{da_+}{dt} = (2ig - \kappa_+)a_+ - \sqrt{2}iG\sigma_- - \sqrt{\frac{\kappa_1}{2}}a_{\text{cw}}^{\text{in}} + \hat{\mathbf{f}}_+, \quad (2)$$

$$\frac{da_-}{dt} = -\kappa_- a_- - \sqrt{\frac{\kappa_1}{2}}a_{\text{cw}}^{\text{in}} + \hat{\mathbf{f}}_-, \quad (3)$$

$$\frac{d\sigma_-}{dt} = -\left(i\Delta_{\text{ec}} + \frac{\gamma_s}{2}\right)\sigma_- + i\sqrt{2}Ga_+\sigma_z + \hat{\mathbf{f}}_1. \quad (4)$$

Here $\sigma_z \equiv |e\rangle\langle e| - |g\rangle\langle g|$, $\Delta_{\text{ec}} \equiv \omega_e - \omega_c$, $\kappa_+ = \kappa_R + (\kappa_0 + \kappa_1)/2$, and $\kappa_- = (\kappa_0 + \kappa_1)/2$; $\kappa_0 = \omega_c/Q_0$ denotes the intrinsic damping of the WGMs with Q_0 being the intrinsic quality factor; κ_1 stands for the cavity-taper coupling strength; $a_{\text{cw}}^{\text{in}}$ is the input field. The operators $\hat{\mathbf{f}}_+$, $\hat{\mathbf{f}}_-$, $\hat{\mathbf{f}}_1$ are the noise operators that conserve the commutation relations at all times. One finds that the symmetric mode a_+ is strongly coupled to the NV center (through dipole interaction) and the nanocrystal (through the scattering), while the antisymmetric mode a_- remains uncoupled to them.

When the cavity is excited by a weak monochromatic field (i.e., weak-field approximation), the NV center is predominantly in the ground state. Thus, σ_z can be substituted for its average value of -1, and Eq. (4) becomes linear. Utilizing the

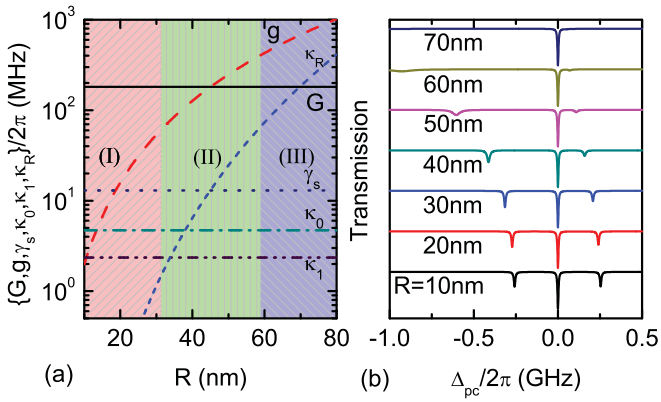

FIG. 2. (Color) (a) Parameters $\{G,g,\gamma_s,\kappa_0,\kappa_1,\kappa_R\}$ as a function of the radius R of the nanocrystal. (b) The transmission spectra for various R. Here $Q_0 = 10^8$, $\kappa_1 = 0.5\kappa_0$, and $\Delta_{\text{ec}} = 0$.

standard input-output formalism $a_m^{\text{out}} = a_m^{\text{in}} + \sqrt{\kappa_1}a_m$ [12], we obtain the outputs

$$a_{\text{cw}}^{\text{out}} = \left[1 + \frac{\kappa_1}{2}\left(\frac{1}{D_+} + \frac{1}{D_-}\right)\right]a_{\text{cw}}^{\text{in}} + \hat{\mathbf{f}}_2', \quad (5)$$

$$a_{\text{ccw}}^{\text{out}} = \frac{\kappa_1}{2}\left(\frac{1}{D_+} - \frac{1}{D_-}\right)a_{\text{cw}}^{\text{in}} + \hat{\mathbf{f}}_3', \quad (6)$$

where $D_+ = i(\Delta_{\text{pc}} + 2g) - \kappa_+ + 2G^2/[i(\Delta_{\text{pc}} - \Delta_{\text{ec}}) - \gamma_s/2]$, $D_- = i\Delta_{\text{pc}} - \kappa_-$, with $\Delta_{\text{pc}} \equiv \omega_p - \omega_c$, and $\hat{\mathbf{f}}_2'$ and $\hat{\mathbf{f}}_3'$ are noise operators. We take the cold reservoir limit where the reservoir modes are all initially in vacuum states. Thus, the expectation values of all noise operators can be neglected because they are annihilated when acting on the initial vacuum states. Then the transmission $\langle a_{\text{cw}}^{\text{out}\dagger}a_{\text{cw}}^{\text{out}}\rangle/\langle a_{\text{cw}}^{\text{in}\dagger}a_{\text{cw}}^{\text{in}}\rangle$ and reflection $\langle a_{\text{ccw}}^{\text{out}\dagger}a_{\text{ccw}}^{\text{out}}\rangle/\langle a_{\text{cw}}^{\text{in}\dagger}a_{\text{cw}}^{\text{in}}\rangle$ can be determined.

Under practical parameters $\gamma_s/2\pi = 13$ MHz, $Q_0 = 10^8$, $\kappa_1 = 0.5\kappa_0$, $V_c \sim 200$ μm^3, and $f_c(\vec{r}) \sim 0.47$, we obtain $\{G,\kappa_0,\kappa_1\}/2\pi \sim \{180,4.7,2.35\}$ MHz. We use these parameters unless otherwise specified. Figure 2(a) plots these parameters depending on the particle radius R. We can approximately divide Fig. 2(a) into three regions. In region I, G far exceeds any other parameters for a small diamond nanocrystal. The NV center couples to the twin WGMs, creating a pair of standing modes. There exist three separate resonance dips in the transmission spectrum: one at the original zero detuning due to the decoupling between the antisymmetric mode and the NV center and the other two split by $2\sqrt{2}G$ due to the strong coupling between the symmetric standing mode and the NV center. The linewidth of the central dip is $\kappa_0 + \kappa_1$; while the linewidths of the two side dips are $\kappa_R + (\kappa_0 + \kappa_1 + \gamma_s)/2$, which can be explained by the dressed state generated by the strong coupling.

With the increase of R, the coefficient g grows rapidly. In region II, g becomes comparable with G, while κ_R is still much smaller than G. The scattering not only moves the two side resonances with detunings $-g \pm (g^2 + 2G^2)^{1/2}$, but also increases their linewidths and decreases the coupling efficiencies. When the size of the nanocrystal is large enough (region III), the scattering damping rate κ_R becomes comparable to or even exceeds G. In this situation, the scattering damping rate is so large that the two side dips nearly vanish. In all cases,

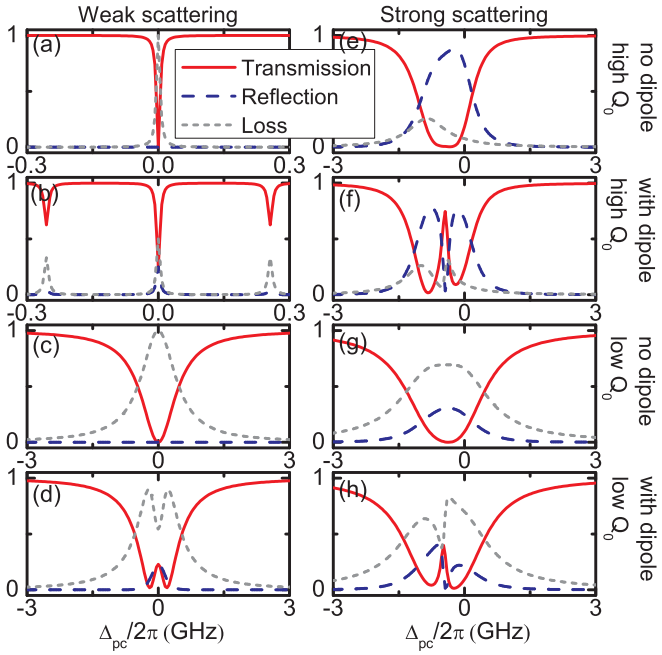

FIG. 3. (Color online) Transmission, reflection, and energy loss of the present system working on the critical coupling point $\kappa_1 = (\kappa_0^2 + 4g^2)^{1/2}$. (a)–(d) Weak-scattering case with $R = 6$ nm and $\Delta_{ec} = 0$. (e)–(h) Strong-scattering case with $R = 60$ nm and $\Delta_{ec} = -g - G^2/g$. The high and low Q_0 are 10^8 and 10^6, respectively.

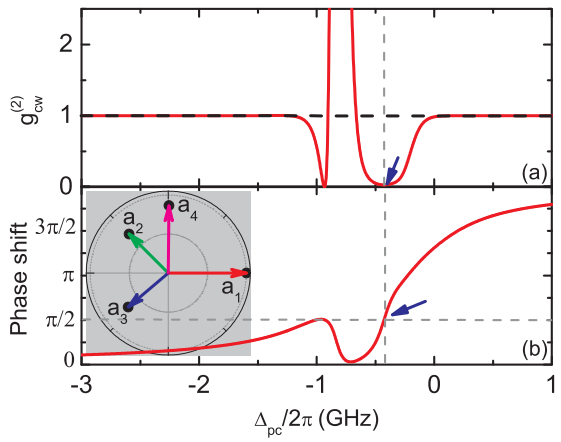

FIG. 4. (Color online) Normalized second-order autocorrelation function $g_{cw}^{(2)}$ (a) and phase shift (b) of the corresponding transmitted field in Fig. 3(f). The dashed vertical lines and blue arrows indicate the position of $\Delta_{pc} = -g$. (Inset) Four components of the transmitted field in the complex plane (see text).

the central dip remains unchanged, and its coupling depends mainly on κ_0 and κ_1.

Transmission spectra for different R varying from 10 to 70 nm are plotted in Fig. 2(b), confirming the above analysis. As the nanocrystal-induced scattering does occur, the new strong-coupling condition requires that $G \gg \{\kappa_+, \gamma_s\}$, corresponding to regions I and II. This provides additional insights into future solid-state CQED.

In the region where the present strong-coupling condition does not apply, interesting DIT effects in the transmission spectrum can be predicted. Let us consider the conditions for the general DIT phenomenon. First, in the absence of the dipole, the new critical coupling condition ($\kappa_1^2 = \kappa_0^2 + 4g^2$) is required to create a relatively broad platform with low transmission. This can be implemented though destructive interference among the directly transmitted field uncoupled to the microcavity and the output field via cavity modes, as discussed in detail in the following. Second, the linewidth of the resonance should be larger than the dipole-cavity coupling strength ($\kappa_+, \kappa_- > G$, i.e., the bad-cavity limit). These conditions are verified in Fig. 3, which presents the transmission, reflection, and energy loss in different conditions.

In the weak-scattering case ($g \ll \kappa_0$), the initial critical coupling condition without dipole is simplified as $\kappa_1 = \kappa_0$. For cavities with high intrinsic quality factor, mode splitting occurs instead of DIT, as shown in Figs. 3(a) and 3(b). This is because the dipole-cavity coupling strength exceeds the resonance linewidth. While a cavity with low intrinsic quality factor can produce DIT as shown in Figs. 3(c) and 3(d), there are significant energy losses, yielding a low DIT peak, as well as low on-off contrast ratio.

In the strong-scattering case ($g \gg \kappa_0$), however, we find that the nanocrystal-induced Rayleigh scattering plays a constructive role in generating DIT and can significantly enhance it, as demonstrated in Figs. 3(e)–3(h). In general, the field radiated by the NV-center dipole takes part in the interference mentioned above. If we control the detuning $\Delta_{ec} = -g - G^2/g$ so that the radiated field intensity has a maximum value at $\Delta_{pc} \simeq -g$ where the initial critical coupling point is located, a DIT window (also at $\Delta_{pc} \simeq -g$) with high efficiency (the peak value exceeds 0.8) appears, because the intrinsic loss is far smaller than the cavity-taper coupling rate ($\kappa_1 \sim 2g \gg \kappa_0$).

High-efficiency DIT holds great potential for photon turnstiles [13,14]. We are thus interested in the photon statistics of the output [15,16], described by the second-order correlation functions $g_m^{(2)} = \langle (a_m^{out\dagger})^2 (a_m^{out})^2 \rangle / \langle a_m^{out\dagger} a_m^{out} \rangle^2$. Figure 4(a) depicts the strong photon antibunching of the transmitted field with a large bandwidth, corresponding to the case in Fig. 3(f). This is because the net transmitted field mainly originates from the NV-center dipole and a single dipole cannot emit two or more photons simultaneously. Actually, excitation of the system by the first photon blocks the transmission of a second photon; this is known as photon blockade [17]. It is of importance that the strong antibunching ($g_{cw}^{(2)} = 0$) occurs exactly at the DIT window, which guarantees the high efficiency of the antibunched light.

In the DIT window, the phase shift ϕ_{cw} of the transmitted field (defined as $\phi_{cw} \equiv \arg[a_{cw}^{out}/a_{cw}^{in}]$) has also been plotted in Fig. 4(b), which exhibits a very large dispersion in the region near $\Delta_{pc} = -g$. This enables us to control the phase shift and group delay of the output field. It is interesting that the transmitted field experiences a $\pi/2$ phase shift at the DIT peak, unlike the previous DIT in [9] (zero shift). To explicitly explain this, from Eq. (5), we note that the transmitted field is an interference of four components: the directly transmitted field uncoupled to the microcavity,

the output field via the antisymmetric mode, the output field via the Rayleigh scattering, and the output field via the NV-center dipole interaction, denoted by $a_{k=1,2,3,4}$, respectively. In the inset of Fig. 4(b) we plot the four components for $\Delta_{pc} = -g$ in the complex plane. Here we find $a_1 = a_{cw}^{in}$ and $a_2 = (\kappa_1/2)a_{cw}^{in}/(i\Delta_{pc} - \kappa_-)$, which cannot be tuned via the nanocrystal; $a_3 = (\kappa_1/2)a_{cw}^{in}/[i(\Delta_{pc} + 2g) - \kappa_+]$ depends on the scattering strength g while a_4 depends mainly on G and Δ_{ec}. It can be seen that a_1, a_2, a_3 destructively interfere, creating zero net field. a_4 has a large amplitude with the relative phase $\pi/2$. This further explains the strong antibunching of the transmitted field in the DIT window.

Finally, in Ref. [13], photon turnstiles are realized by coupling a microcavity to a single cold cesium atom. Standing wave modes built there are induced by scattering from defects and surface roughness of the microtoroidal cavity, and thus photon turnstiles are sensitive to the atom's azimuthal position. Averaging over the azimuthal angle results in a significant reduction of the on-off contrast ratio of transmission in the DIT window [see Fig. 1(E) in Ref. [13]]. In the present Rapid Communication, Rayleigh scattering is induced by the diamond nanocrystal itself. Thus, these devices are almost immune to the azimuthal position of the nanocrystal. This is of special importance when multiple nanocrystals are involved in the microcavity system. For example, the dynamics of the coupling system will strongly depend on the interpositions of these nanocrystals.

In summary, we have analyzed a single diamond nanocrystal with a NV center coupled to high-Q counterpropagating twin WGMs of a microtoroidal cavity. It is found that the Rayleigh scattering induced by the nanocrystal itself not only induces strong interaction between the twin WGMs, but also results in scattering loss of the WGMs. This provides further insight into future solid-state CQED. We also reveal that Rayleigh scattering can play a positive role in obtaining DIT with high efficiency, accompanying strong photon antibunching. The system can perform as a photon turnstile which is almost immune to the azimuthal position of the nanocrystal. Our investigation can be of practical use in controlled interactions of single quanta and scalable quantum logic.

Note added. Recently, a related publication [18] appeared.

This work was supported by the NSFC (Grants No. 10821062, No. 11004003, and No. 11023003) and the 973 program (Grant No. 2007CB307001). Yun-Feng Xiao was also supported by the Research Fund for the Doctoral Program of Higher Education (Grant No. 20090001120004) and the Scientific Research Foundation for Returned Overseas Chinese Scholars.

[1] H. Mabuchi and A. C. Doherty, Science **298**, 1372 (2002).
[2] G. Khitrova, H. M. Gibbs, M. Kira, S. W. Koch, and A. Scherer, Nat. Phys. **2**, 81 (2006).
[3] V. B. Braginsky, M. L. Gorodetsky, and V. S. Ilchenko, Phys. Lett. A **137**, 393 (1989).
[4] N. Le Thomas *et al*., Nano Lett. **6**, 557 (2006); Y.-S. Park *et al*., *ibid*. **6**, 2075 (2006); S. Schietinger, T. Schroder, and O. Benson, *ibid*. **8**, 3911 (2008).
[5] E. Peter *et al*., Phys. Rev. Lett. **95**, 067401 (2005); T. Aoki *et al*., Nature (London) **443**, 671 (2006); K. Srinivasan and O. Painter, *ibid*. **450**, 862 (2007); K. Srinivasan, C. P. Michael, R. Perahia, and O. Painter, Phys. Rev. A **78**, 033839 (2008); J.-T. Shen and S. Fan, *ibid*. **79**, 023838 (2009).
[6] T. Gaebel *et al*., Nat. Phys. **2**, 408 (2006).
[7] F. Jelezko *et al*., Phys. Rev. Lett. **93**, 130501 (2004); R. J. Epstein, F. M. Mendoza, Y. K. Kato, and D. D. Awschalom, Nat. Phys. **1**, 94 (2005); M. V. Gurudev Dutt *et al*., Science **316**, 1312 (2007).
[8] P. E. Barclay, C. Santori, K.-M. Fu, R. G. Beausoleil, and O. Painter, Opt. Express **17**, 8081 (2009).
[9] E. Waks and J. Vuckovic, Phys. Rev. Lett. **96**, 153601 (2006).
[10] D. K. Armani, T. J. Kippenberg, S. M. Spillane, and K. J. Vahala, Nature (London) **421**, 925 (2003).
[11] A. Mazzei *et al*., Phys. Rev. Lett. **99**, 173603 (2007); J. Zhu *et al*., Nat. Photon. **4**, 46 (2010).
[12] C. W. Gardiner and P. Zoller, *Quantum Noise*, 3rd ed. (Springer, Berlin, 2004).
[13] B. Dayan *et al*., Science **319**, 1062 (2008).
[14] K. Srinivasan and O. Painter, Phys. Rev. A **75**, 023814 (2007).
[15] H. J. Carmichael, *Statistical Methods in Quantim Optics 2: Non-classical Fields* (Springer, Berlin, 2008).
[16] H. J. Carmichael, Phys. Rev. Lett. **55**, 2790 (1985).
[17] A. Imamoglu, H. Schmidt, G. Woods, and M. Deutsch, Phys. Rev. Lett. **79**, 1467 (1997).
[18] H. Uys *et al*., Phys. Rev. Lett. **105**, 200401 (2010).